Received: 16 July 2019 | Revised: 25 October 2019 | Accepted: 29 October 2019

DOI: 10.1002/glia.23751

GLIA

WILEY

RESEARCH ARTICLE

Limited contribution of astroglial gap junction coupling to buffering of extracellular K^+ in CA1 stratum radiatum

Björn Breithausen[1] | Steffen Kautzmann[1] | Anne Boehlen[1] | Christian Steinhäuser[1] | Christian Henneberger[1,2,3]

[1]Institute of Cellular Neurosciences, University of Bonn Medical School, Bonn, Germany

[2]Institute of Neurology, University College London, London, UK

[3]German Center for Neurodegenerative Diseases (DZNE), Bonn, Germany

Correspondence
Christian Henneberger, Institute of Cellular Neurosciences, University of Bonn Medical School, Bonn, Germany.
Email: christian.henneberger@uni-bonn.de

Funding information
Deutsche Forschungsgemeinschaft, Grant/Award Numbers: HE6949/1, HE6949/3, HE6949/4, SFB1089 B03, STE552/4; EU Marie Skłodowska-Curie Actions; NRW-Rückkehrerprogramm

Abstract

Astrocytes form large networks, in which individual cells are connected via gap junctions. It is thought that this astroglial gap junction coupling contributes to the buffering of extracellular K^+ increases. However, it is largely unknown how the control of extracellular K^+ by astroglial gap junction coupling depends on the underlying activity patterns and on the magnitude of extracellular K^+ increases. We explored this dependency in acute hippocampal slices (CA1, stratum radiatum) by direct K^+-sensitive microelectrode recordings and acute pharmacological inhibition of gap junctions. K^+ transients evoked by synaptic and axonal activity were largely unaffected by acute astroglial uncoupling in slices obtained from young and adult rats. Iontophoretic K^+-application enabled us to generate K^+ gradients with defined spatial properties and magnitude. By varying the K^+-iontophoresis position and protocol, we found that acute pharmacological uncoupling increases the amplitude of K^+ transients once their initial amplitude exceeded ~10 mM. Our experiments demonstrate that the contribution of gap junction coupling to buffering of extracellular K^+ gradients is limited to large and localized K^+ increases.

KEYWORDS

astrocytes, gap junctions, hippocampus, K^+ buffering, K^+ clearance, K^+ homeostasis, K^+-sensitive microelectrodes

1 | INTRODUCTION

Extracellular K^+ is involved in many processes in the brain. Its concentration determines, for instance, neuronal excitability and thereby neuronal activity levels. At the same time, extracellular K^+ levels are increased by neuronal activity. It is therefore intuitive that the extracellular K^+ concentration ($[K^+]_O$) is tightly controlled by various mechanisms and that their failure can contribute to diseases such as epilepsy (de Curtis, Uva, Gnatkovsky, & Librizzi, 2018; Kofuji & Newman, 2004). Especially astrocytes, an electrically unexcitable glial cell type, have a repertoire of cellular mechanisms that can clear and/or buffer $[K^+]_O$ increases. Direct uptake of K^+ by the Na^+/K^+-ATPase, for example, has been demonstrated to play a major role in K^+ clearance in the hippocampus (D'Ambrosio, Gordon, & Winn, 2002; Xiong & Stringer, 2000) and astrocytes contribute to that (Karus, Mondragão, Ziemens, & Rose, 2015; Larsen et al., 2014).

Another important astrocytic mechanism is spatial buffering of extracellular K^+ increases: The redistribution of extracellular K^+ from sites of high extracellular concentrations to tissue with lower extracellular K^+ levels via the astrocytic cytosol (Kofuji & Newman, 2004; Newman, Frambach, & Odette, 1984). It is thought that K^+ entry into the astrocytic cytosol at sites of high extracellular K^+ is mainly

facilitated by inwardly rectifying K^+ channels. There is broad experimental evidence that Kir4.1 is expressed by astrocytes, sets their membrane potential and mediates a substantial part of their K^+ currents in the hippocampus in vitro and in vivo (Chever, Djukic, McCarthy, & Amzica, 2010; Djukic, Casper, Philpot, Chin, & McCarthy, 2007; Seifert et al., 2009; Sibille, Pannasch, & Rouach, 2014) and that Kir4.1 shapes directly recorded extracellular K^+ transients (Haj-Yasein et al., 2011; Larsen et al., 2014). According to the spatial buffering concept, K^+ is then redistributed within the cytosol of individual astrocytes and the large networks astrocytes formed by gap junction coupling (Giaume, Koulakoff, Roux, Holcman, & Rouach, 2010; Kofuji & Newman, 2004; Larsen & MacAulay, 2014). These gap junctions, which are formed between adjacent cells but also between processes of the same astrocyte (Genoud, Houades, Kraftsik, Welker, & Giaume, 2015; Giaume et al., 2010), facilitate K^+ diffusion and, importantly, electrically couple regions of astrocytes exposed to high extracellular K^+ to those at rest. They can thereby maintain a membrane potential more negative than the equilibrium potential of K^+ at sites of high extracellular K^+, which is needed for local K^+ uptake (Kofuji & Newman, 2004). Removal of gap junctions is therefore expected to increase the amplitude and to possibly slow down the decay of extracellular K^+ transients. However, to what extent this mechanism shapes K^+ transients and determines K^+ clearance has remained a matter of debate.

Knockout of the connexins (Cx) that form gap junctions in hippocampal astrocytes (Cx43 and Cx30) completely abolished astrocyte coupling in the hippocampus, strongly altered synaptic transmission and plasticity, neuronal excitability and promoted epileptiform activity in the hippocampus and, indeed, mildly increased the amplitude and slowed the decay of K^+ transients (Pannasch et al., 2011; Wallraff et al., 2006). However, knockout of Cx30 has more recently been demonstrated to alter fine astrocyte morphology and excitatory synapse function (Pannasch et al., 2014) and polarization of hippocampal astrocytes (Ghézali et al., 2018), which could alter K^+ signals independent of gap junction dependent buffering. Similarly, increased astroglial dye coupling in aquaporin 4 knockout mice was associated with smaller K^+-transients in response to stimulation of CA1 pyramidal cells but slower restoration of the resting K^+ (Strohschein et al., 2011) and inactivation of the *Tsc1* gene reduced astroglial gap junction coupling and increased the amplitude of K^+ transients (Xu, Zeng, & Wong, 2009). Again, these studies provide important insights into the effects of gene deletion but cannot ascertain that the effects on K^+ transients are directly related to changes of spatial K^+ buffering and not secondary to other effects of gene deletion. Acute blockade of gap junctions using carbenoxolone (CBX) in the cortex increases the extracellular K^+ concentration in vivo and reduces evoked somatosensory field responses (Bazzigaluppi, Weisspapir, Stefanovic, Leybaert, & Carlen, 2017). However, in addition to off-target effects of CBX (Ransom, Ye, Spain, & Richerson, 2017; Tovar, Maher, & Westbrook, 2009; Vessey et al., 2004) this could have been due to closure of gap junctions in neurons and/or astrocytes, the latter also affecting metabolite shuttling (Clasadonte, Scemes, Wang, Boison, & Haydon, 2017; Rouach, Koulakoff, Abudara, Willecke, & Giaume, 2008; Zsiros & Maccaferri, 2005). It has also been suggested that CBX and Cx43 deletion inhibit hemichannels thereby modulating synaptic transmission (Chever, Lee, & Rouach, 2014; Meunier et al., 2017). This could in turn affect extracellular K^+ signals caused by synaptic activity independently of gap junction dependent spatial K^+ buffering.

Overall, these reported results unequivocally establish important mechanistic links between gap junctions and various aspects of brain function. They also highlight the experimental challenges of clearly identifying the contribution of astrocytic gap junction coupling to spatial K^+ buffering. To obtain further insights, we examined the effect of acute pharmacological gap junction uncoupling on extracellular K^+ transients recorded using K^+-sensitive microelectrodes, mainly in the CA1 stratum radiatum of acute hippocampal slices. These K^+ transients were evoked by stimuli that were themselves not sensitive to gap junction inhibitors (e.g., iontophoretic injection of K^+ during inhibited neuronal activity). Over a wide range of stimulation protocols, the detected effects of gap junction closure on extracellular K^+ transients were limited to locally induced K^+ transients with amplitudes of >10 mM. This suggests that the contribution of astrocytic gap junction coupling to spatial K^+ buffering is mainly confined to pathological conditions.

2 | METHODS

2.1 | Animals and slice preparation

Acute hippocampal slices were obtained as described previously (Anders et al., 2014; Minge et al., 2017). Briefly, acute hippocampal slices were obtained from 3- to 5- and 8- to 10-week old Wistar rats (Charles River) in full compliance with national and institutional guidelines on animal experimentation. Slices were cut to a thickness of 300 and 350 μm for patch-clamp experiments and K^+ measurements, respectively, horizontally in an ice-cold slicing solution containing (in mM): NaCl 60, sucrose 105, KCl 2.5, $MgCl_2$ 7, NaH_2PO_4 1.25, ascorbic acid 1.3, sodium pyruvate 3, $NaHCO_3$ 26, $CaCl_2$ 0.5 and glucose 10 (300–310 mOsm), and kept in that solution at 34°C for 15 min before being stored at room temperature (21–23°C) in an extracellular solution containing (in mM) NaCl 126, KCl 3, $MgSO_4$ 1.3, NaH_2PO_4 26, $CaCl_2$ 2 and glucose 10 (297–303 mOsm). All solutions were constantly bubbled with 95% O_2/5% CO_2. Slices were allowed to rest for at least 30 min before recording started.

2.2 | Quantification of astroglial gap junction coupling by dye-loading

The strength of astroglial gap junction coupling was determined by fluorescent dye loading via a whole-cell patch pipette and visualization of dye spread in the astroglial network by two-photon excitation fluorescence microscopy, as described previously (Anders et al., 2014). For recordings, hippocampal slices were transferred to a submersion-type recording chamber and superfused with extracellular solution at 34°C. Whole-cell recordings from CA1 astrocytes in the stratum radiatum were performed using standard patch-pipettes

(3.5–4.5 MΩ) filled with an intracellular solution containing (in mM) KCH_3O_3S 135, HEPES 10, di-Tris-Phosphocreatine 10, $MgCl_2$ 4, Na_2-ATP 4, Na-GTP 0.4 (pH adjusted to 7.2 using KOH, osmolarity 290–295 mOsm). In two subsets of recordings, 50 μM carbenoxolone (CBX) or 100 μM meclofenamic acid (MFA) were added to the extracellular solution 10 min before dye loading began by establishing the whole-cell patch clamp configuration. For visualization of the astrocyte morphology and astroglial gap junction coupling, Texas Red Dextran 3 kDa (300 μM, Invitrogen) and Alexa Fluor 488 hydrazide (80 μM, Invitrogen) were added to the intracellular solution, respectively. Astrocytes were identified by their small soma, characteristic morphology, passive whole-cell current pattern and their highly negative resting membrane potential.

For the visualization of astrocyte morphology and gap junction coupled astroglial networks, we used a two-photon excitation fluorescence microscope (Scientifica, UK) optically linked to a femtosecond pulse laser (Coherent Vision S, λ = 800 nm) equipped with a 40× objective (NA 0.8). The laser power was corrected for recording depth to obtain 2 mW at the patched cell. For the analysis of gap junction coupling, an image stack was obtained (512 × 512 pixels, 323.8 × 323.8 μm, variable number of slices 2 μm apart) 10 min after establishing the whole-cell configuration, thus allowing Alexa Fluor 488 to spread through the gap junction coupled network for 10 min. The access resistance was monitored throughout the whole-cell patch-clamp experiments. Experiments were discarded if the initial access resistance was above 35 MΩ. Although access resistance increased gradually during experiments it was not affected by CBX or MFA treatment, neither initially (control: 18.04 ± 2.97 MΩ, n = 7, CBX: 19.37 ± 4.63 MΩ, n = 5; p = .81, two-sample Student's t test; control: 10.32 ± 0.72 MΩ, n = 7, MFA: 12.18 ± 1.54 MΩ, n = 5; p = .25, two-sample Student's t test) nor after 10 min dye-dialysis (control: 23.4 ± 3.7 MΩ, n = 7, CBX: 23.53 ± 5.1 MΩ, n = 5, p = .92, two-sample Student's t test; control: 17.4 ± 1.69 MΩ, n = 7, MFA: 21.2 ± 1.71 MΩ, n = 5, p = .16, two-sample Student's t test). The evaluation of the gap-junction coupled network was performed using ImageJ (NIH) as previously described (Anders et al., 2014). Briefly, the background fluorescence intensity was subtracted for the entire image stack and the results were corrected for depth. Gap junction coupled cells were identified manually and their somatic fluorescence intensity was normalized to the somatic intensity of the patched astrocyte. Cells were discarded from analysis if their normalized fluorescence intensities were below 1% of the patched cell, to prevent inclusion of ambiguous cells and other faintly fluorescent structure (e.g., autofluorescence). The number of coupled cells (without the patched astrocyte) and their cumulative fluorescence intensity was used as measures of the strength of gap junction coupling.

2.3 | Construction of K^+-sensitive microelectrodes and extracellular $[K^+]$ measurements

The fabrication of the K^+ sensitive microelectrodes was adapted from (Uwe Heinemann & Dieter Lux, 1977; Lux & Neher, 1973; Wallraff et al., 2006). Briefly, K^+-sensitive microelectrodes were built using theta-glass capillaries (Hilgenberg) and pulled with a horizontal pipette puller (P-87; Sutter Instruments Co.). The reference and the K^+-sensitive barrel were filled with a NaCl (154 mM) and KCl (150 mM) solutions, respectively. The tip of the K^+-sensitive barrel was filled with a valinomycin-based K^+ ionophore (K^+ ionophore 1, cocktail A or B, Sigma-Aldrich) after silanization with a mixture of dichloromethane (1984 μl, Sigma-Aldrich) and trimethylchlorosilane (94.5 μl, Sigma-Aldrich, St. Louis, MO). Ag/AgCl wires were inserted in both barrels, sealed with wax and connected to the headstage of the differential amplifier (ION-01M; npi). The K^+-sensitive microelectrodes were calibrated before each experiment with solutions containing 154 mM NaCl and 3 or 30 mM KCl and displayed an average voltage response (V_C) of 55.5 ± 0.18 mV (n = 124) to a tenfold increase of $[K^+]$. The voltage response obtained during calibration was used to convert the measured signals (V) into K^+ concentrations using the following relationship: $[K^+] = 10\ \hat{}\ (V/V_C + \log_{10}[K^+]_0)$ where $[K^+]_0$ is the extracellular K^+ resting concentration of 3 mM. The K^+ transients measured with the two different K^+-selective ionophores (cocktail A and B) showed no difference in their peak amplitude (p = .48, Mann–Whitney U test), rise time (p = .11, Mann–Whitney U test) and decay (fast time constant, p = 1.00, Mann–Whitney U test; slow time constant, p = .292, two-sample Student's t test; fast decaying fraction, p = .606, two-sample Student's t test; slowly decaying fraction, p = .561, two-sample Student's t test) and were therefore pooled for analysis. A clear undershoot following evoked K^+ transients was only observed in a small minority of experiments and therefore not analyzed.

Slices were transferred to an interface-type chamber and superfused with extracellular solution at 34°C for recording of K^+ transients induced by neuronal activity. A bipolar stimulation electrode was placed in the stratum radiatum at the CA3/CA1 border to stimulate Schaffer collaterals. The evoked neuronal activity and K^+ transients were recorded with a standard patch pipette filled with extracellular solution (EXT-02B, npi, Germany; USB-6221, National Instruments) and a K^+-sensitive microelectrode in the CA1 stratum radiatum (ION-01 M npi, Germany; USB-6221, National Instruments) respectively, and stored for offline analysis. K^+ transients were either evoked by paired-pulse stimulation (50 ms interstimulus interval) or a high-frequency stimulation (HFS, 50 pulses at 100 Hz) in the presence of the ionotropic glutamate receptor blockers NBQX (10 μM) and D-APV (50 μM). The stimulation intensity was adjusted to obtain 75% of the maximum field excitatory postsynaptic potential (fEPSP) amplitude for the paired-pulse stimulation and of maximal fiber volley amplitudes for the HFS.

A submersion-type recording chamber was used for recording of iontophoretically induced K^+ transients from acute slices superfused with extracellular solution at 34°C. These experiments were performed in the presence of TTX (1 μM), NBQX (10 μM), and D-APV (50 μM) to silence neuronal activity. K^+ transients were recorded in the stratum radiatum and lacunosum moleculare of the CA1 region with K^+-sensitive microelectrodes (ION-01M, npi, Germany; Digidata 1440A, Molecular Devices, Eugene, OR) and stored for offline

analysis. Iontophoretic application of K^+ (MVCS-02C, npi, Germany) was used to create a defined K^+ point source and K^+ transients. K^+ transients with low and high amplitudes were induced via *weak* and *strong* current injections (Figure 5) through iontophoresis pipettes filled with 150 mM KCl (800 nA for 200 ms, 15 s interval, *weak* K^+ pulse) and 3 M KCl (900 nA for 500 ms, 45 s interval, *strong* K^+ pulse), respectively. For experiments with K^+ transients of variable peak amplitudes (Figure 6c,d), iontophoresis pipettes were filled with 3 M KCl and K^+ was applied at an interval of 20 s with different injection currents and durations. A constant retain-current of −5 to −15 nA was applied to avoid K^+ leakage from the iontophoresis pipette. Iontophoresis pipettes filled with 150 mM and 3 M KCl exhibited resistances of 50–120 MΩ and 8–12 MΩ, respectively.

Drugs and compounds were purchased from Sigma (MFA, CBX, and D-APV) and Abcam (D-APV, TTX, and NBQX). Microelectrodes and capillaries were purchased from Hilgenberg (Germany) and Science Products (Germany).

2.4 | Data analysis and statistics

All data are presented as mean ± standard error of mean (SEM). Statistical significance was evaluated with Origin (OriginLab, Northampton, MA) using paired and unpaired Student's *t* test if data followed a normal distribution (Shapiro–Wilk test), Wilcoxon signed-rank tests, and Mann–Whitney *U*-tests and ANOVA as indicated. Significance levels are indicated in the figures by asterisks (*p < .05, **p < .01, ***p < .001) and provided in the text and/or figure legends. "*n*" refers to the number of experiments. We performed one experiment per brain slice throughout the study. On average, we obtained about 1–2 successful slice recordings per animal. In pharmacological experiments, an initial *baseline* was routinely recorded before a drug was applied. The baseline value is the average of the baseline data points. *Drug/control* recordings refer to those where drug/no drug was applied and the effect was quantified at the end of the recording (typically average of last 2–3 min, same averaging time window within sets of control/drug experiments).

3 | RESULTS

The role of astroglial gap junction coupling for buffering of extracellular K^+ was tested by acute inhibition of gap junctions using carbenoxolone (CBX) or meclofenamic acid (MFA). We first established to what extent astroglial gap junction coupling is reduced by bath application of CBX (50 μM) or MFA (100 μM) for 10 min in acute hippocampal slices under our experimental conditions. Astroglial gap junction coupling was quantified in dye coupling experiments using a combination of two-photon excitation fluorescence microscopy and whole-cell patch clamp, as described previously (Anders et al., 2014; Henneberger & Rusakov, 2012). In these experiments, CBX or MFA were acutely applied via the extracellular solution. After 10 min of drug application an astrocyte was loaded with the gap junction permeable fluorescent dye Alexa Fluor 488 and the gap junction impermeable Texas Red Dextran 3 kDa (to visualize only the loaded cell) via the whole-cell patch clamp pipette (Figure 1a). An image stack capturing the spread of Alexa Fluor 488 into the gap junction-coupled astroglial network was obtained after 10 min of dye loading and analyzed (Figure 1b). For both gap junction inhibitors, the number of coupled cells was reduced (Figure 1c,d). Similarly, both gap junction inhibitors strongly decreased the cumulative fluorescence intensity of coupled cells (Figure 1c,d, CBX by 96.9% and MFA by 85.2%). Because the cumulative fluorescence intensity is not a direct measure of coupling between individual cells in the astroglial network, we reproduced these measurements using a previously published model of astroglial coupling (Anders et al., 2014). In this model, diffusion between individual astrocytes in the network is described by a single diffusion constant, which we adjusted to match the cumulative fluorescence intensity after simulated dye filling to experimental data in control conditions, in CBX and in MFA (right panels of Figure 1c,d). We found that our present results can be explained by a near-complete inhibition of coupling between astrocytes (by 97.7% in CBX and 86.5% in MFA, not illustrated).

3.1 | K^+ transients evoked by synaptic and axonal activity

If the clearance of K^+ from extracellular space is supported by astroglial gap junction coupling, an increase of K^+ transient amplitudes or a change of their decay is expected when the coupling is disrupted. This hypothesis was first tested on K^+ transients that result from synaptic activity driven by stimulation of CA3–CA1 Schaffer collaterals. Excitatory field potentials (fEPSPs) and the accompanying K^+ transients were simultaneously recorded in the hippocampal CA1 stratum radiatum (Figure 2a,c) and the stimulation intensity was set so that fEPSP had a slope of 75% of the maximum. After recording of a baseline period, gap junction coupling was inhibited by bath application of MFA for 10 min. We chose MFA for these experiments because MFA is a potent and reversible inhibitor of gap junctions (Harks et al., 2001; Pan, Mills, & Massey, 2007) with relatively few reports of side effects in the literature. Indeed, bath application of MFA did not affect the fEPSP slope in slices from 3- to 5- and 8- to 10-week-old animals (not illustrated; young animals: p = .55, n = 7, Wilcoxon signed-rank test; older animals: p = .31, n = 5, paired Student's t test). We next combined MFA application, recording of fEPSPs and monitoring of K^+ transients using K^+-sensitive microelectrodes in experiments in hippocampal slices from juvenile animals (age of 3–5 weeks). No effect of MFA bath application on the amplitude and decay of K^+ transients could be detected (Figure 2c,d). Because the mechanisms controlling extracellular K^+ homeostasis (e.g., extracellular space, K^+ channel expression, Na/K-ATPase expression) could still further mature into adulthood, we also performed experiments on slices from adult animals (8–10 weeks). Again, application of MFA had no significant effect on the amplitude and decay of K^+ transients. This indicates that acute uncoupling of astrocytes by MFA does not alter the K^+ transients

caused by synaptic activity that was induced by a commonly used stimulation paradigm. Because these K^+ transients had relatively small amplitudes of ~0.1 mM, they may not have been large enough to be controlled by astroglial gap junction coupling.

Therefore, we next investigated larger K^+ transients with an amplitude of ~0.5 mM, which were elicited by high-frequency stimulation of CA3–CA1 Schaffer collaterals (Figure 3a,b, HFS, 50 pulses at 100 Hz) in the presence of glutamate receptor inhibitors to prevent uncontrolled changes of the stimulated cells and tissue (e.g., synaptic plasticity). Again, gap junction inhibition did not affect the neuronal response (i.e., the fiber volley amplitude), the K^+ transient amplitude or its decay in slices from juvenile animals (Figure 3c). In contrast, the amplitudes of both the fiber volley and the K^+ transient were increased when the experiments were performed in slices from adult animals (Figure 3d). There are two potential explanations of this observation. First, uncoupling of astrocytes indeed impairs K^+ clearance, which leads to higher K^+ transient amplitudes, thereby increased axonal excitability during the HFS and in turn higher fiber volley amplitudes. Second, CBX could increase axonal excitability independent of gap junction coupling, thereby increasing recruitment of axons by electrical stimulation and thus leading to increased fiber volley and K^+ transient amplitudes. Indeed, CBX was shown to have a variety of gap junction-independent effects on neurons including broadening of action potentials (Rouach, Segal, Koulakoff, Giaume, & Avignone, 2004; Tovar et al., 2009; Vessey et al., 2004). In order to differentiate between these two scenarios, we next performed experiments using iontophoretic K^+ application to generate a defined K^+ source.

3.2 | Probing extracellular K^+ dynamics using an iontophoretic K^+ point source

Iontophoretic K^+ application has several advantages for the generation of K^+ transients over the approaches used above. It creates a single K^+ point source with known location. It also avoids biases introduced by effects of gap junction inhibitors on processes such as

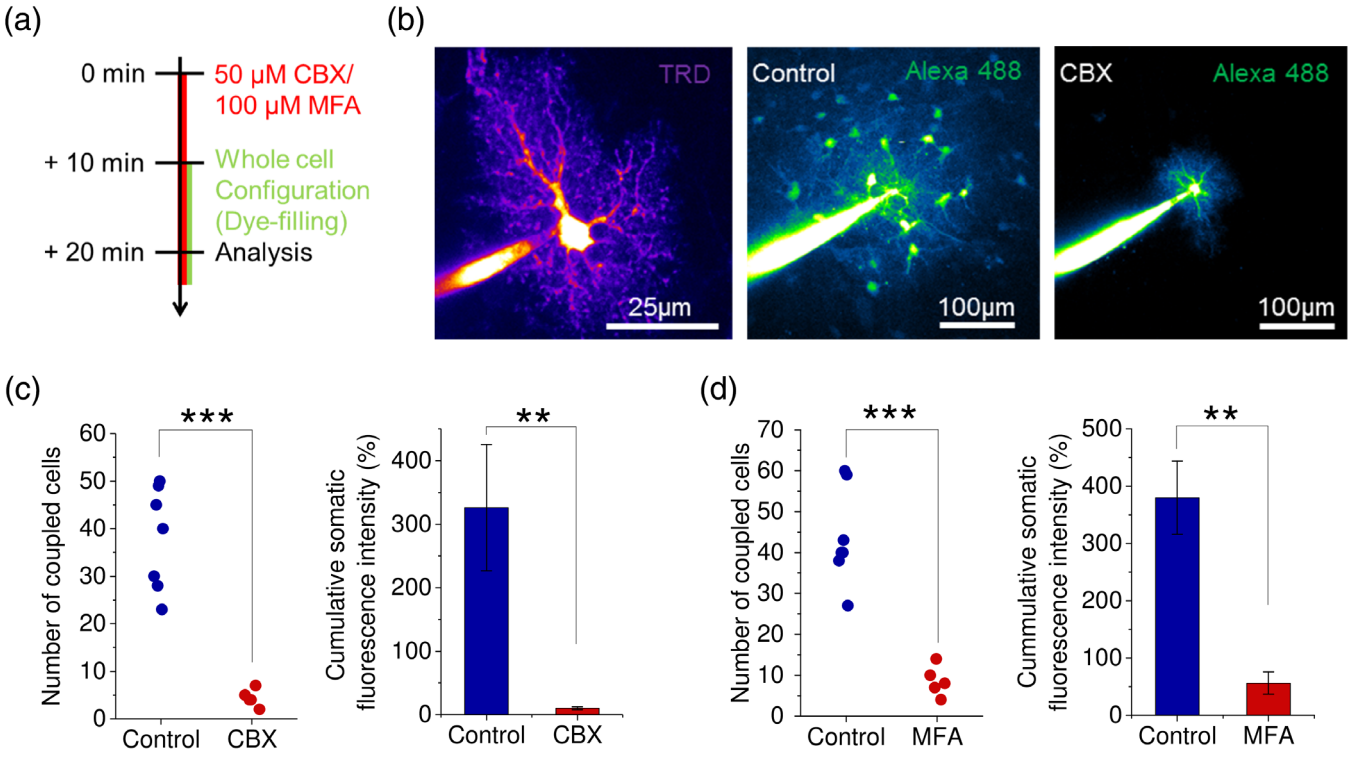

FIGURE 1 Rapid disruption of astroglial dye coupling by the gap junction inhibitors CBX and MFA. (a) Schematic time-course of the experiment. Hippocampal slices were treated with carbenoxolone (CBX, 50 µM) or meclofenamic acid (MFA, 100 µM) for 10 min. Next, an astrocyte was patched and loaded with fluorescent dyes Alexa Fluor 488 (gap junction permeable) and Texas Red Dextran (3 kDa, gap junction impermeable, for visualization of the patched cell). After 10 min an image stack was obtained and the astrocyte dye-coupling was analyzed. (b) Left panel: A typical patched astrocyte (Texas Red Dextran 3 kDa, TRD, 300 µM). Middle panel: Dye-coupling in the astroglial network under control conditions after 10 min dye-loading (Alexa Fluor 488, 80 µM) into a single astrocyte held in whole-cell configuration. Right panel: Same as middle, but after 10 min treatment with CBX. (c) Compared to control recordings, CBX reduced the number of dye-coupled cells (control: 37.85 ± 4.10, n = 7, CBX: 4.40 ± 0.81, n = 5; p < .001, two-sample Student's t test) and their cumulative normalized somatic fluorescence intensity compared to control condition (control: 326.04 ± 99.37%, n = 7; CBX: 10.18 ± 2.37%, n = 5; p = .00568, Mann–Whitney Test). (d) Compared to control recordings, MFA reduced the number of dye-coupled cells (control: 43.9 ± 4.47, n = 7, MFA: 8.60 ± 1.66, n = 5; p < .001, two-sample Student's t test) and their cumulative normalized somatic fluorescence intensity (control: 397.4 ± 63.8%, n = 7, MFA: 56.3 ± 20.0%, n = 5; p = .00181, two-sample Student's t test)

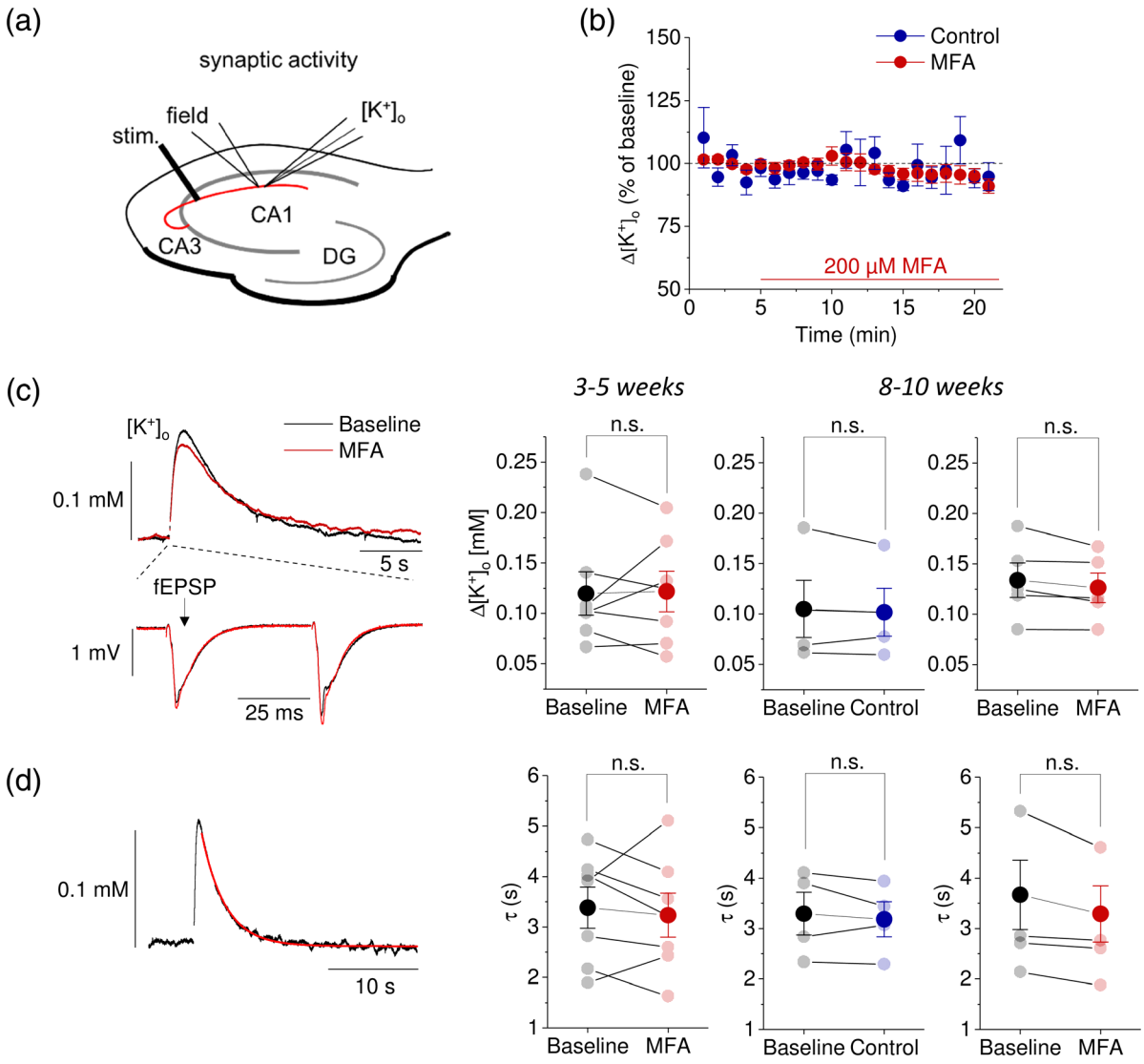

FIGURE 2 No effect of uncoupling of astroglia using MFA on K^+ transients evoked by synaptic activity in two age groups. (a) Schematic of experimental approach for evoking and recording CA3–CA1 synaptic activity and simultaneous monitoring of K^+ transients in the hippocampal CA1 stratum radiatum (K^+, K^+-sensitive microelectrode; field, field recording electrode; stim., stimulation electrode). Recording electrodes were positioned closely together. Paired pulses with an interstimulus interval of 50 ms were required to elicit K^+ transients with amplitudes of ~0.1 mM. (b) Time course of extracellular K^+ transients ($\Delta[K^+]_O$) in control (blue) and during wash-in of MFA (red, 200 µM, slices from 8- to 10-week-old animals). See panel c for sample responses. (c) Examples of simultaneously recorded extracellular K^+ transients (left top panel) and excitatory field potentials (fEPSP, left bottom panel). Superimposed trace from baseline (black) and after 10–15 min of MFA application (red). Summary of experiments with MFA application (red) and control experiments (blue) in slice obtained from 3- to 5- and 8- to 10-week-old animals as indicated (paired Student's *t* tests; from left to right: p = .93, .57, .12 and n = 7, 4, 5). (d) The decay phase of synaptically evoked K^+ transient was best approximated by a monoexponentially decaying function (left panel, fit superimposed in red). Summary of decay time constants in experiments with MFA application (red) and control experiments (blue) as in c (paired Student's *t* test; from left to right: p = .61, .50, .056 and n = 7, 4, 5)

action potential firing and synaptic transmission. In addition, the amount of K^+ that is injected into the extracellular space is easily controlled by the iontophoretic current amplitude and duration. To establish these recordings, we combined iontophoretic K^+ application with measurements of K^+ transients at a defined distance (see Figure 4a for an example) and characterized basic spatial properties of the evoked transients. In this type of experiment, TTX (1 µM), NBQX (10 µM), and D-APV (50 µM) were always added to the extracellular solution to inhibit action potential firing and glutamatergic synaptic transmission. This blocks network activity, including its potential changes by K^+-iontophoresis, and the resulting activity-dependent release of K^+ into the extracellular space but may leave some depolarization-dependent mechanisms intact.

The amplitude of the recorded K^+ transients decreased as the distance of the recording electrode increased. This relationship could be approximated by a monoexponentially decaying function (Figure 4b)

with an overall decay constant of 13.08 ± 0.79 μm (n = 22; CA1 stratum lacunosum moleculare: 9.47 ± 1.52, n = 3, not illustrated). We next tested if this decay is direction-dependent (anisotropic) for two reasons. First, extracellular diffusion of ions is shaped by the structure of the extracellular space (ECS) and the ECS tortuosity in the hippocampus has been shown to be anisotropic and favoring diffusion along the trajectory of CA3–CA1 Schaffer collaterals (Mazel, Sčimonová, & Syková, 1998; Syková & Vargová, 2008). Second, we have previously shown that astroglial morphology and gap junction coupling is anisotropic in CA1 stratum radiatum favoring coupling in parallel to CA1 pyramidal cell dendrites (Anders et al., 2014), which suggests that propagation of extracellular K^+ transients may be anisotropic if gap junction coupling is relevant for K^+ buffering. We therefore tested in paired experiments if iontophoretically induced K^+ transients decay differently along these axes, that is, in parallel and perpendicular to the CA1 pyramidal cells layer. However, no significant direction-dependency could be detected (Figure 4c and figure legend).

3.3 | Effect of astrocyte uncoupling on iontophoretically induced K^+ transients

We then asked what the effect of astroglial uncoupling on iontophoretically induced extracellular K^+ transients is. First, we used an iontophoresis protocol that created weak K^+ pulses, monitored K^+ transients over a baseline period and then acutely inhibited gap junctions by bath application of CBX as before (Figure 5a,b). No effect of CBX was detected on the amplitudes of K^+ transients (Figure 5c, initial amplitudes in control: 2.18 ± 0.56 mM, n = 14; in CBX: 2.30 ± 0.71 mM, n = 16; p = .723, Mann–Whitney U test) and on their decay time constant (Figure 5d, initial decay time constants in control: 1.68 ± 0.326 s, n = 13; in CBX: 2.20 ± 0.301 s, n = 15; p = .251, two-sample Student's t test).

Next, we tested if acute gap junction blockade impacts larger extracellular K^+ transients induced by stronger K^+ pulses. This was achieved by increasing the iontophoretic current to 900 nA and its duration to 0.5 s. Again, 50 μM CBX was bath-applied after recording of a baseline period. Compared to control experiments, application of CBX increased the amplitude of these K^+ transients significantly (Figure 5e–g, initial amplitudes in control: 9.25 ± 1.65 mM, n = 15; in CBX: 8.28 ± 1.62 mM, n = 20; p = .516, Mann–Whitney U test). In contrast, the decay of K^+ transients was not affected by CBX (Figure 5h, initial fast decay time constants (τ_{fast}) in control: 1.05 ± 0.102 s, n = 15; in CBX: 1.20 ± 0.115 s, n = 19; p = .349, two-

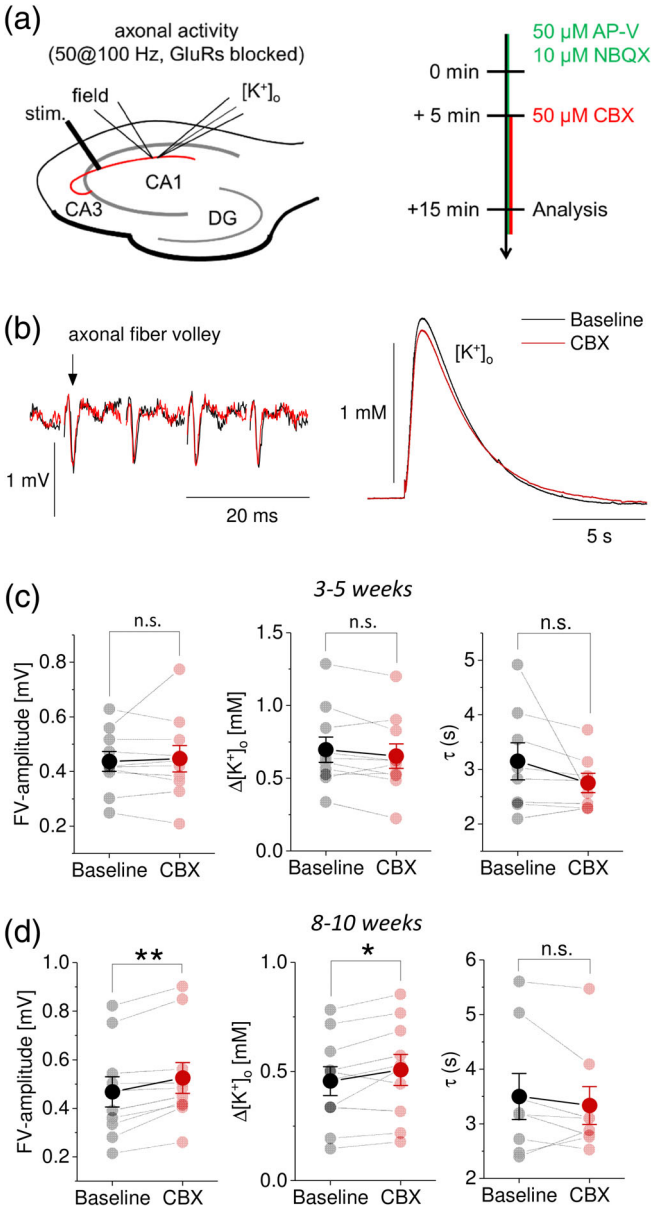

FIGURE 3 Effects of uncoupling of astroglia using CBX on K^+ transients evoked by axonal activity in two age groups. (a) Schematic of experimental approach for evoking and recording CA3–CA1 Schaffer collateral activity using high-frequency stimulation (HFS, 50 pulses at 100 Hz every minute) and simultaneous monitoring of K^+ transients in the hippocampal CA1 stratum radiatum (left panel; KSM, K^+-sensitive microelectrode; field, field recording electrode; stim., stimulation). Recording electrodes were positioned closely together. Timeline of experiments (right panel). Experiments were performed in the presence of the glutamate receptor antagonists NBQX and D-APV as indicated. (b) Representative recording of axonal fiber volleys (left panel, initial four fiber volleys) during baseline (black) and after 10–15 min of CBX application (red). The corresponding K^+ transients are shown in the right panel. (c) Statistical summary of experiments in acute slices obtained from 3-5-week-old animals. Application of CBX had no statistically significant effect on the axonal fiber volley amplitude (FV), the amplitude of HFS-induced K^+ transients and their decay in slices from younger animals (paired Student's t test; from left to right: p = .685, .109, .198 and n = 10, 10, 10). (d) Statistical summary of experiments in acute slices obtained from 8- to 10-week-old animals. In this age group, CBX increased the FV and K^+ transient amplitude but did not significantly affect K^+ transient decay (paired Student's t-test for left and middle panel: p = .00138 and .0299, Wilcoxon signed-rank test for right panel: p = .232, n = 10 throughout)

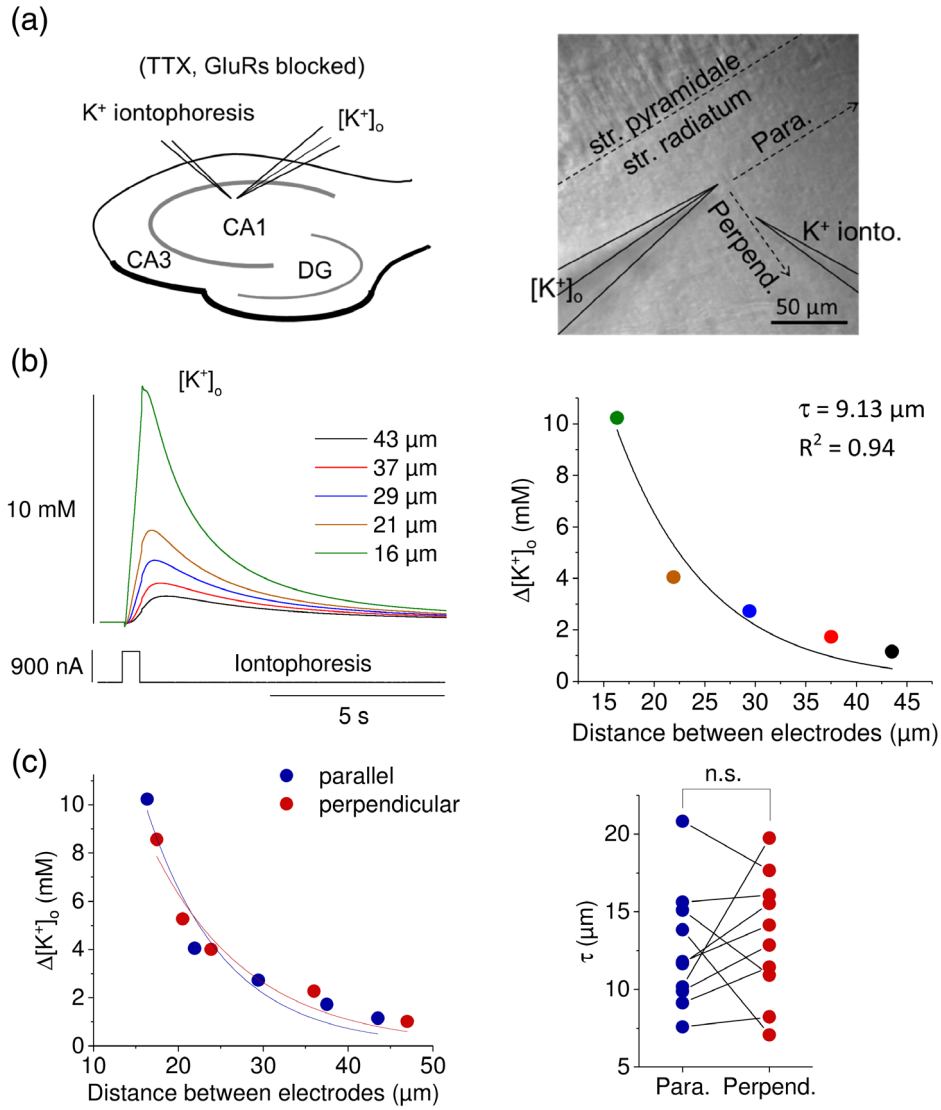

FIGURE 4 Spatial propagation of ionotophoretically evoked K^+ transients. (a) Schematic (left panel) and Dodt contrast camera image (right panel) of experimental arrangement (KSM, K^+-sensitive microelectrode; Ionto., iontophoresis pipette). A K^+ point source was created by iontophoretic injection of K^+ at different distances relative to the K^+-sensitive microelectrode. The iontophoresis pipette was moved either parallel or perpendicular to the stratum pyramidale (str. pyramidale). (b) Example of iontophoretically evoked K^+ transients (current amplitude 900 nA, duration 0.5 s) recorded at different distances from the K^+-sensitive microelectrode as illustrated (left panel). The amplitude of K^+ transients decreased monoexponentially with distance (right panel). (c) Example of the distance-dependence of K^+ transient in parallel with the stratum pyramidale (blue) and perpendicular to the pyramidal cell layer from a single experiment (red, left panel). The K^+-sensitive electrode was kept in place for the entire experiment whereas the K^+-iontophoresis pipette was moved successively closer to the K^+-sensitive electrode. The distance-dependent decline of the K^+ transient peak amplitude was not significantly different in parallel and perpendicular to the str. pyramidale (parallel 12.6 ± 1.23 µm, perpendicular 13.4 ± 1.28 µm, n = 10 experiments and slices from seven animals, p = .60, paired Student's t test). In addition to the spatial decay of peak amplitudes, we also analyzed the spatial decay of K^+ concentrations 2 and 5 s after the K^+ injections, that is, in the falling flank of the K^+ transients, in both directions. Again, no statistically significant difference was observed between the decay in parallel and perpendicular to the str. pyramidale (2 s, p = .66; 5 s, p = .87, n = 10 both, paired Student's t tests)

sample Student's t test and initial slow decay time constants (τ_{slow}) in control: 6.22 s ± 0.535 s, n = 15; in CBX: 6.79 ± 0.648 s, n = 19; p = .503, two-sample Student's t test). Despite the lack of an effect of CBX on the decay phase we observed across the entire data set that the fast decaying component became more prominent with increasing peak amplitudes and that both the fast and slow decay constant decreased with increasing amplitudes (Spearman rank tests: percentage of fast component, ρ = .36; p = .0024; fast decay constant, ρ = −.86, p < .0001; slow decay constant, ρ = −.70, p < .0001) as reported by previous studies (Ransom, Ransom, & Sontheimer, 2000; Wallraff et al., 2006).

These observations suggest that astroglial gap junction coupling may selectively control large K^+ transients. However, the locally recorded amplitude of K^+ transients does not only depend on the

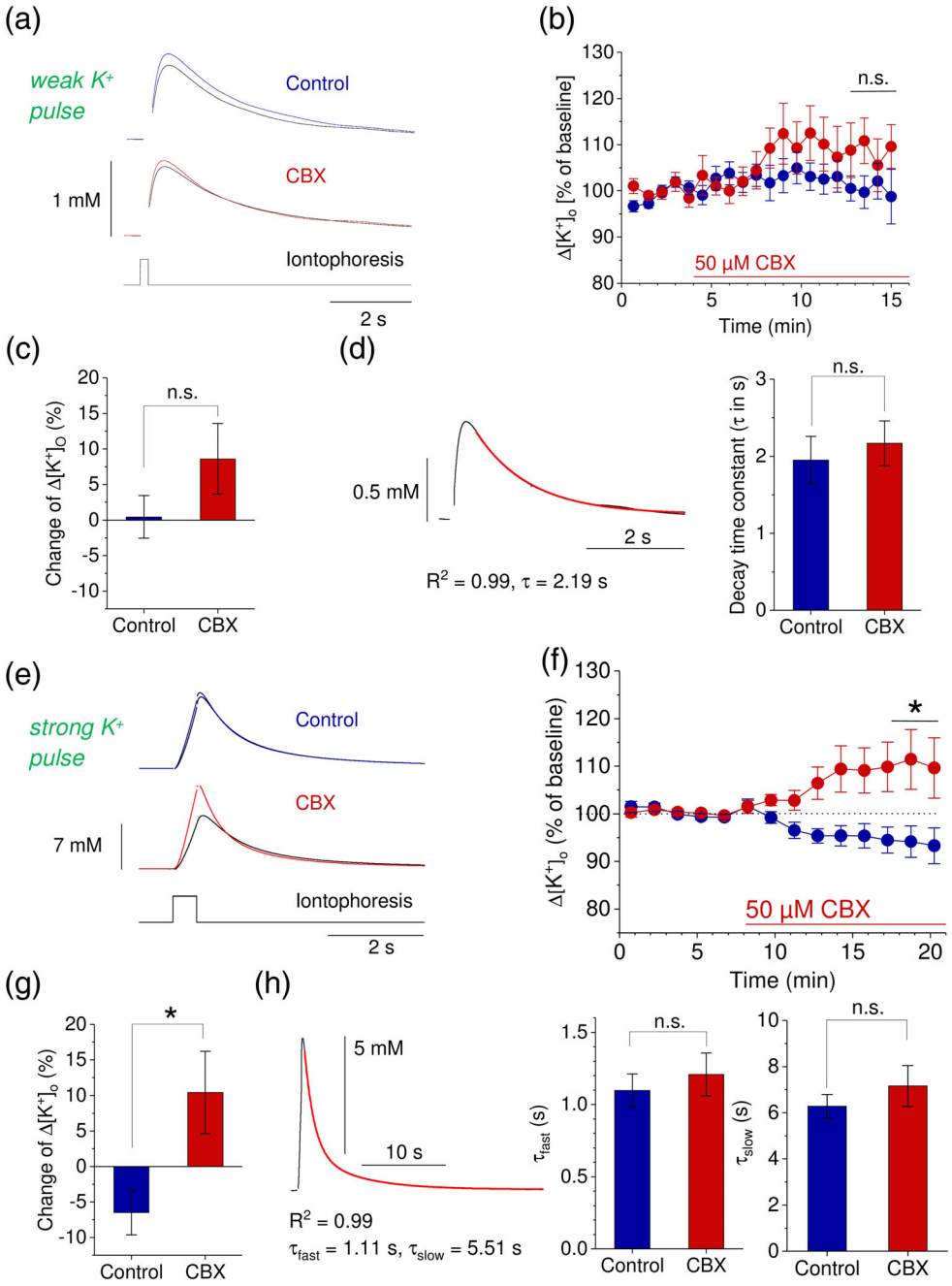

FIGURE 5 Selective increase of large K^+ transients by gap junction uncoupling using CBX. Two sets of experiments using weak and strong protocols of ionotophoretic K^+ application (a–d and e–f, respectively). (a) Examples of K^+ transients evoked by weak iontophoretic injections of K^+ (800 nA for 0.2 s, "weak K^+ pulse"). Sample control experiment in top panel (baseline in black, superimposed control in blue). Individual CBX experiments middle panel (baseline in black, superimposed trace after 10 min of CBX application in red). (b) Time course of K^+ transient peak amplitudes normalized to the baseline period (control in blue, CBX in red). Red line indicates period of CBX bath application. (c) Relative change of the K^+ transient amplitudes after CBX application compared to control (control: 0.42 ± 2.99%, n = 14; CBX: 8.60 ± 4.97%, n = 16; p = .606, two-sample Student's t-test, averaged over the time period indicated by black horizontal line in b). (d) The decay of the K^+ transients evoked by weak K^+ pulses was best approximated by a monoexponentially decaying function (red line). The decay time constant was not different at the end of control and CBX experiments (control: 1.94 ± 0.31 s, n = 13; CBX: 2.16 ± 0.29 s, n = 15 both; p = .61; two-sample Student's t test). (e) Example transients evoked by strong iontophoretic injections of K^+ (900 nA for 0.5 s, "strong K^+ pulse") illustrated as in a. (f) Time course of K^+ transient peak amplitudes normalized to the baseline period (control in blue, CBX in red). Red line indicates period of CBX bath application. (g) Relative change of the K^+ peak amplitudes after CBX-treatment compared to control (control: –6.47 ± 3.13%, n = 15; CBX: 10.41 ± 5.78%, n = 20; p = .0244 Mann–Whitney test, averaged over the time period indicated by black horizontal line in f). (h) The decay of the "high" amplitude K^+ transients was best approximated by biexponentially decaying functions (red line). Significant differences between control and CBX experiments were detected neither in the fast component (control: 1.10 ± 0.114 s, n = 15; CBX 1.21 ± 0.149 s, n = 19; p = .559, two-sample Student's t test) nor in the slow (control: 6.28 ± 0.514 s; CBX: 7.16 ± 0.885 s; p = .835, Mann–Whitney U test)

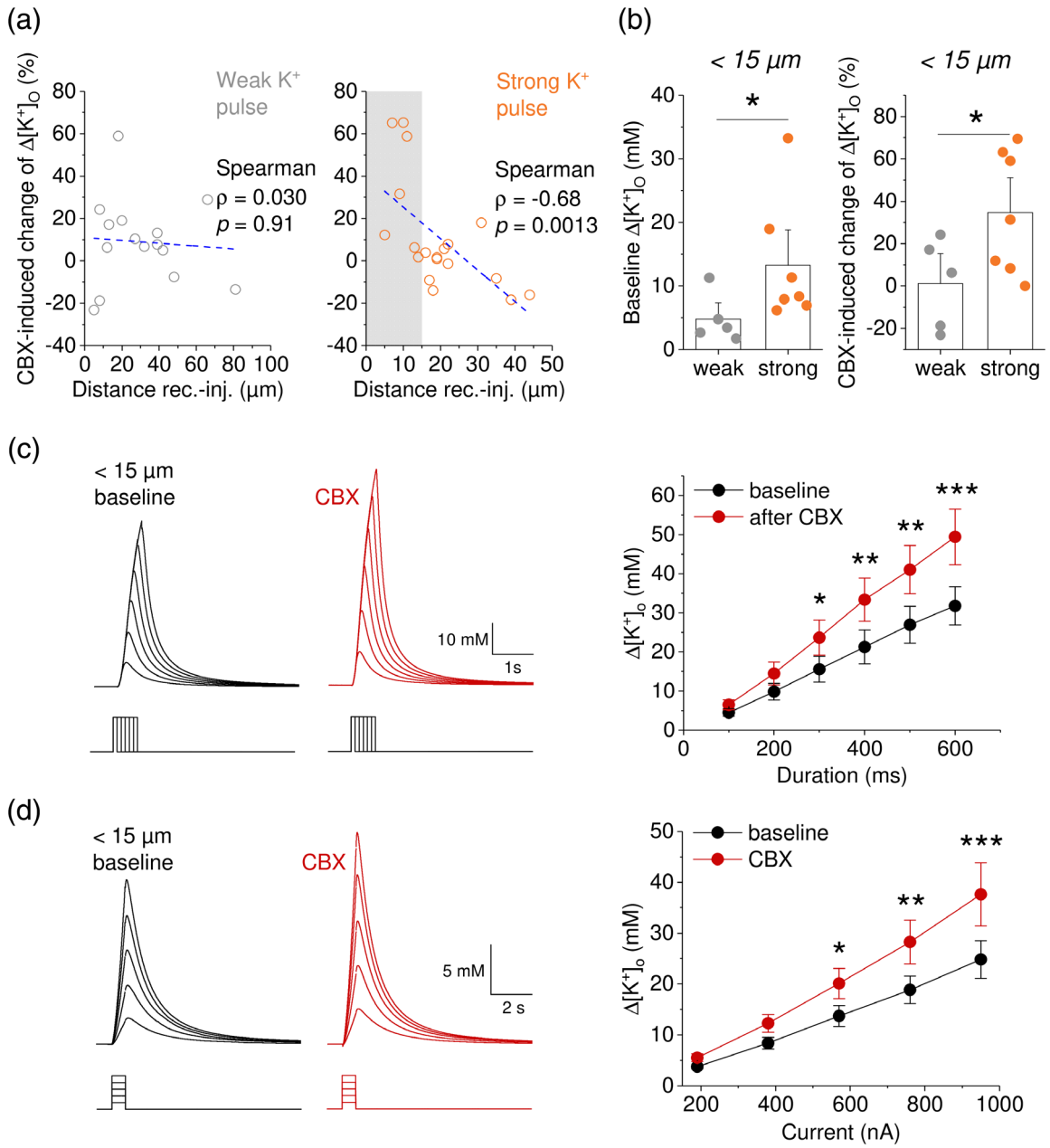

FIGURE 6 Gap junction uncoupling increases K^+ transients with high amplitude. (a) The effect of CBX on amplitudes of K^+ transients evoked by *weak* K^+ pulses was not correlated with the distance between the sites of iontophoretic K^+ injection and K^+ recording (left panel, data from Figure 5a–d, control experiments omitted, $n = 15$, dashed line represents linear fit for illustration). In contrast, a significant correlation was detected between the distance and the CBX effect on K^+ transients evoked by *strong* K^+ pulses (right panel, data from Figure 5e–h, control experiments omitted, $n = 19$, dashed line represents linear fit for illustration). The CBX-induced increase of K^+ transients is prominent when recordings were made close to the K^+ injection site. (b) To reveal if either amplitude or distance determines the CBX effect, we selected recordings made at a distance of less than 15 µm (from a, only CBX recordings, weak and strong K^+ pulses). Intuitively, the baseline amplitude of K^+ transients evoked by *weak* K^+ pulses was lower than the amplitudes of transients evoked by *strong* K^+ pulses (left panel, $p = .0487$, unpaired Student's *t* test). Similarly, the magnitude of the CBX effect was significantly higher on K^+ transients evoked by *strong* K^+ pulses (right panel, $p = .0430$; two-sample Student's *t* test, <15 µm) although recordings were made at similar distance (see text). Additionally, a significant effect of CBX was only detected on transients evoked by *strong* but not *weak* K^+ pulses (strong: 34.7 ± 10. 9%, $p = .0192$, $n = 7$; weak: 1.15 ± 9.49, $n = 5$, $p = .909$; one-sample Student's *t* tests). (c) Testing the dependency of the CBX effect on the duration of K^+ injection at distances between the recording electrode and the K^+ injection electrode below 15 µm. A set of current durations from 100 to 600 ms (900 nA) were tested before (baseline) and after CBX application. Starting at a duration of 300 ms CBX significantly increased the amplitudes of K^+ transients (two-way repeated measures ANOVA, *p* for interaction of duration and CBX < .001, *p* for CBX = .0443, $n = 5$, Holm–Bonferroni correction in *post hoc* tests). (d) Similarly, the dependence on the iontophoretic current amplitude was tested (190–950 nA, 500 ms). A significant effect of CBX was observed at 570 nA and above (two-way repeated-measures ANOVA, *p* for interaction of current amplitude and CBX < .001, *p* for CBX = .0223, $n = 10$, Holm–Bonferroni correction in *post hoc* tests)

amount of injected K^+ but also on the distance to the site of injection (Figure 4). To dissect how amplitude and distance shape the CBX effect of K^+ transients, we first correlated the CBX effect with the distance between K^+ injection and recording sites. For recordings obtained with weak K^+ pulses, which showed no overall effect of CBX, no significant correlation was found (Figure 6a, left panel). In contrast, we observed a highly significant negative correlation between distance and CBX effect when strong K^+ pulses were used (Figure 6a, right panel). The increase of the K^+ transient amplitude after CBX application was prominent in these experiments at distances less than 15 μm (Figure 6a, right panel, grey bar), that is, close to the K^+ injection site where K^+ transients are large.

To identify if either recording distance or the K^+ transient amplitude determines if CBX has an effect, we next compared the CBX effect of recordings using weak and strong K^+ pulses at short, similar distances. We first compared the baseline amplitudes from CBX recordings with weak and strong K^+ pulses at distances less than 15 μm (strong K^+ pulse: 9.86 ± 1.20 μm, n = 7; weak K^+ pulse: 9.20 ± 1.46, n = 5; p = .737; two-sample Student's t test) and found that, intuitively, strong K^+ pulses led to higher amplitudes of extracellular K^+ transients (Figure 6b, left panel). Importantly, there was virtually no CBX effect on K^+ transients in response to weak K^+ pulses, in contrast to strong K^+ pulse at these similar distances (Figure 6b, right panel). These observations demonstrate that acute gap junction uncoupling increases the amplitude of large, local K^+ transients. This conclusion is further supported by a positive correlation between baseline K^+ transient amplitude and the CBX effect in pooled data (Spearman rank correlation, ρ = 0.678, p = .0153, n = 12, distance <15 μm). We then varied the amplitude and duration of iontophoretic K^+ injections to obtain further information about the relationship between K^+ transient amplitude and the effect of gap junction closure. In both sets of experiments, a statistically significant increase of K^+ transients by CBX was observed once the baseline K^+ transients exceeded an amplitude of ~10–15 mM (Figure 6c,d). Importantly, the ramps of K^+ injections themselves did not significantly affect the amplitude of K^+ transients (amplitude before vs. after ramps, p = .313, n = 6, Wilcoxon's signed rank test, not illustrated). Finally, we tested if the amplitudes of large localized K^+ transients (K^+ ionotophoresis, 900 nA, 500 ms, distance 18.0 ± 1.73 μm, n = 4) are also increased by the gap junction inhibitor MFA. This was indeed the case (increase by 29.6 ± 7.5%, n = 4, p = .034, paired Student's t test, not illustrated).

Investigating the decay of K^+ transients across all conditions, we found again that the fast decaying component became more dominant and the decay time constants decreased as the amplitude increased (fast decay component fraction, ρ = 0.19, p = .047; fast decay constant, ρ = −0.71, p < .0001; slow decay constant, ρ = −0.51, p < .0001; Spearman rank correlations). Although the CBX-application did not significantly affect the relative magnitude of the fast decay component (p = .37, two-way repeated-measures ANOVA, data from Figure 6d) it did decrease the fast and slow decay time constants overall (fast: p = .045 for CBX, slow: p = .013 for CBX, two-way repeated measures ANOVA, no significant interactions between stimulation intensity and CBX effect, not illustrated). To test if this reduction of the decay time constants is a consequence of higher K^+ transient amplitudes after uncoupling, we pooled K^+ transients before and after CBX application, grouped the pooled transients before and after CBX application according to their amplitudes and then compared the decay time constants before and after CBX in each group. No statistically significant difference was found (five amplitude groups, fast time constant p = .98, slow time constant p = .20, two-way ANOVA) indicating that the more rapid decay of K^+ transients after CBX is a consequence of their higher amplitudes.

4 | DISCUSSION

We have analyzed to what extent extracellular K^+ transients triggered by a range of different stimuli are affected by acute disruption of astroglial gap junction coupling in the CA1 area of the hippocampus. The latter was achieved in our experiments by pharmacological inhibition of gap junctions with CBX and MFA, which resulted in near-complete inhibition of astroglial gap junction coupling. We found that synaptic and axonal activity patterns widely used in electrophysiological tests of hippocampal circuit function evoked robust extracellular K^+ transients, directly recorded by K^+-sensitive microelectrodes, with amplitudes ranging from ~0.1 to 1 mM. However, neither the amplitude nor the kinetics of these K^+ transients was altered after blockade of gap junctions in acute hippocampal slices obtained from 3- to 5-week-old and adult rats. Our observations indicate that astroglial gap junction coupling does not contribute to the clearance of extracellular K^+ in these conditions and these ranges of K^+ concentration increases.

There are at least two possible explanations. First, the stimulation of axons and synapses could lead to a global and relatively homogeneous increase of extracellular K^+ instead of the spatial K^+ gradient required for spatial buffering. Second, the induced activity patterns could lead to sparse and short-range K^+ increases in the vicinity of active axons, synapses, and/or dendrites that are widely distributed. Therefore, such small and localized extracellular K^+ transients might dissipate and be cleared by other mechanisms (see section 1) on a spatial scale to which gap junction dependent processes do not contribute significantly. Further and more detailed insights into these processes cannot be obtained using K^+-sensitive microelectrodes because they sample a single point of such K^+ landscapes with unknown distance to the site of K^+ transient generation. This obstacle might be overcome in the future by the use of newly developed optical K^+ sensors (P. Bazzigaluppi, Dufour, & Carlen, 2015; Bischof et al., 2017; Wellbourne-Wood, Rimmele, & Chatton, 2017), which could be useful for monitoring small transients, their spatial extent and their control by gap junctions. Independent of these considerations, our experiments do not provide evidence for a role of gap junctions in controlling K^+ transients in these concentration ranges and in recording and stimulation paradigms widely used in electrophysiological test of hippocampal function.

To reliably evoke stronger K^+ transients, we next used iontophoretic K^+ application in the presence of a drug cocktail silencing neurons, which creates a defined K^+ point source with known location in the tissue. This is advantageous in the context of our experiments because it isolates the effect of gap junction inhibition on K^+ buffering and clearance and avoids effects of gap junction blockade on the mechanisms that generate the K^+ transients (see Introduction). We first characterized the distance-dependency of K^+ transients evoked by this method and found that the peak amplitude decreased with a decay constant of ~10–15 μm. It is unlikely that this measure is affected by the constant flow of extracellular solution to which the entire slice surface is exposed to because our average recording depth of ~50–100 μm is much larger than the measured decay constant of ~10–15 μm. In vivo this space constant could be different, because blood vessels, surrounded by strongly gap junction coupled astrocyte endfeet (Nagy, Patel, Ochalski, & Stelmack, 1999; Simard, Arcuino, Takano, Liu, & Nedergaard, 2003), are the main K^+ sink. We then tested whether the spatial spread of K^+ transients is anisotropic. This could be expected because we and others have previously shown that gap junction coupling is anisotropic in the CA1 stratum radiatum (Anders et al., 2014; Ghézali et al., 2018). However, such anisotropy of K^+ transient spread was not observed.

Further experiments revealed that gap junction inhibition significantly increased the amplitude of extracellular K^+ transients once amplitudes reached ~10–15 mM. This indicates that the contribution of gap junctions to clearance of extracellular K^+ transients is limited to strong K^+ elevations generally associated with pathophysiological conditions (de Curtis et al., 2018; U. Heinemann, Lux, & Gutnick, 1977; Somjen, 2001). This is reminiscent of previous experiments in hippocampal slices from mice lacking the astroglial Cx43 and Cx30 and thus astroglial gap junction coupling. In these animals, K^+ transients were mildly increased in the CA1 stratum pyramidale and decreased in CA1 stratum lacunosum moleculare only with maximum stimulation of CA1 pyramidal cell axons and repetitive stimulation (Wallraff et al., 2006). Therefore, smaller, more physiological K^+ elevations are not shaped by gap junction dependent mechanism in CA1 stratum radiatum. Of course, this does not rule out a role of spatial buffering for these small K^+ elevations in general, for example, via Kir4.1. However, it should be noted that evidence for Kir4.1-dependent spatial K^+ buffering has been obtained using large K^+ transients induced by repetitive strong synaptic stimulation (Haj-Yasein et al., 2011) or large spatial K^+ gradients using iontophoretic K^+ injections (Larsen et al., 2014). Given that astrocytes are heterogenous in structure, function and coupling across brain regions (Griemsmann et al., 2015; Matyash & Kettenmann, 2010; Zhang & Barres, 2010) the degree to which gap junctions contribute to K^+ buffering is also likely to vary between brain regions and their sublayers.

The decay of K^+ transients was not slowed by gap junction uncoupling in any of our experiments. Instead, the decay phase was accelerated when gap junction uncoupling increased the amplitude of K^+ transients. This is in line with and expected from our and previous observations (Strohschein et al., 2011; Wallraff et al., 2006), which show that the decay of K^+ transients is accelerated as the amplitude increases under control conditions. The previously observed slowing of K^+ transients in slices with Cx43/30-deficient astrocytes could have been caused by the changes of fine astrocyte process morphology or reduced morphological polarity demonstrated for Cx-deficient astrocytes in CA1 stratum radiatum (Ghézali et al., 2018; Pannasch et al., 2014). Overall, our observation that K^+ transient decay was not slowed by gap junction blockade is in line with the general idea that the return of extracellular K^+ to its baseline after neuronal activity is largely mediated by Na^+/K^+-ATPases (D'Ambrosio et al., 2002; Larsen et al., 2014; Ransom et al., 2000) and that it is not substantially affected by spatial buffering via, for instance, Kir4.1 (Larsen et al., 2014; Larsen & MacAulay, 2014).

Our results raise the question under which conditions astroglia gap junction coupling contributes to the regulation of extracellular K^+ increases. According to our results that would be the case when K^+ gradients higher than about ~10 mM are being generated, which can occur in vivo during maximal stimulation of the brain or during epileptic activity (U. Heinemann et al., 1977; Sypert & Ward, 1974). Interestingly, the abundant gap junction coupling found between astrocytes in human control tissue is completely absent in patients with pharmacoresistant temporal lobe epilepsy (Bedner et al., 2015) in CA1 stratum radiatum. This suggests that failure of gap junction dependent K^+ redistribution in these patients may exacerbate epileptic activity. Furthermore, it has been shown that spatially highly confined epileptic activity plays an important role in seizure initiation and propagation (Schevon et al., 2008; Wenzel, Hamm, Peterka, & Yuste, 2019). It appears probable that such local activity can generate the large K^+ gradients required for K^+ redistribution via astrocytic gap junctions.

Strong spatial K^+ gradients are also generated at the wave front of a spreading depression (Somjen, 2001) and gap junction-mediated spatial buffering of K^+ could therefore dampen the build-up of extracellular K^+ at the wave front and slow down wave front propagation. Indeed, deletion of Cx43 from hippocampal astrocytes, which resulted in reduced gap junction coupling between hippocampal astrocytes, increased the propagation velocity of spreading depression in hippocampal slices (Theis et al., 2003). Thus, in line with our present observation astrocytic gap junction coupling does contribute to phenomena, in which strong K^+ increases occur. It is also conceivable that similarly high K^+ concentration gradients could be transiently reached if extracellular space shrinks or large amounts of K^+ are very locally released into small extracellular compartments (e.g., during synaptic transmission). Future experiments could test if, when and where such steep spatial K^+ gradients occur and if they are modulated by astrocytic gap junction coupling.

ACKNOWLEDGEMENTS

We thank Uwe Heinemann (Berlin, Germany) and Christine Rose (Düsseldorf, Germany) for excellent advice on K^+-sensitive electrode recordings. The work was supported by the NRW-Rückkehrerprogramm (to C.H.), the European Union Marie Sklodowsksa-Curie Actions (ITN EU-GliaPhD to C.H. and C.S.) and the German Research Foundation (DFG; SFB1089 B03, SPP1757 HE6949/1, HE6949/3, HE6949/4 to C.H.; STE552/4 to C.S.).

CONFLICT OF INTEREST

The authors declare that they have no conflict of interest.

DATA AVAILABILITY STATEMENT

The data that support the findings of this study are available from the corresponding author upon reasonable request.

ORCID

Christian Steinhäuser https://orcid.org/0000-0003-2579-8357
Christian Henneberger https://orcid.org/0000-0002-5391-7387

REFERENCES

Anders, S., Minge, D., Griemsmann, S., Herde, M. K., Steinhäuser, C., & Henneberger, C. (2014). Spatial properties of astrocyte gap junction coupling in the rat hippocampus. *Philosophical Transactions of the Royal Society, B: Biological Sciences*, *369*(1654), 20130600. https://doi.org/10.1098/rstb.2013.0600

Bazzigaluppi, P., Dufour, S., & Carlen, P. L. (2015). Wide field fluorescent imaging of extracellular spatiotemporal potassium dynamics in vivo. *NeuroImage*, *104*, 110–116. https://doi.org/10.1016/j.neuroimage.2014.10.012

Bazzigaluppi, P., Weisspapir, I., Stefanovic, B., Leybaert, L., & Carlen, P. L. (2017). Astrocytic gap junction blockade markedly increases extracellular potassium without causing seizures in the mouse neocortex. *Neurobiology of Disease*, *101*, 1–7. https://doi.org/10.1016/j.nbd.2016.12.017

Bedner, P., Dupper, A., Hüttmann, K., Müller, J., Herde, M. K., Dublin, P., … Steinhäuser, C. (2015). Astrocyte uncoupling as a cause of human temporal lobe epilepsy. *Brain*, *138*(5), 1208–1222. https://doi.org/10.1093/brain/awv067

Bischof, H., Rehberg, M., Stryeck, S., Artinger, K., Eroglu, E., Waldeck-Weiermair, M., … Malli, R. (2017). Novel genetically encoded fluorescent probes enable real-time detection of potassium in vitro and in vivo. *Nature Communications*, *8*(1), 1422. https://doi.org/10.1038/s41467-017-01615-z

Chever, O., Djukic, B., McCarthy, K. D., & Amzica, F. (2010). Implication of Kir4.1 channel in excess potassium clearance: An in vivo study on anesthetized glial-conditional Kir4.1 Knock-out mice. *The Journal of Neuroscience*, *30*(47), 15769–15777. https://doi.org/10.1523/JNEUROSCI.2078-10.2010

Chever, O., Lee, C.-Y., & Rouach, N. (2014). Astroglial Connexin43 Hemichannels tune basal excitatory synaptic transmission. *The Journal of Neuroscience*, *34*(34), 11228–11232. https://doi.org/10.1523/JNEUROSCI.0015-14.2014

Clasadonte, J., Scemes, E., Wang, Z., Boison, D., & Haydon, P. G. (2017). Connexin 43-mediated Astroglial metabolic networks contribute to the regulation of the sleep-wake cycle. *Neuron*, *95*(6), 1365–1380.e5. https://doi.org/10.1016/j.neuron.2017.08.022

D'Ambrosio, R., Gordon, D. S., & Winn, H. R. (2002). Differential role of KIR Channel and Na^+/K^+-pump in the regulation of extracellular K^+ in rat hippocampus. *Journal of Neurophysiology*, *87*(1), 87–102. https://doi.org/10.1152/jn.00240.2001

de Curtis, M., Uva, L., Gnatkovsky, V., & Librizzi, L. (2018). Potassium dynamics and seizures: Why is potassium ictogenic? *Epilepsy Research*, *143*, 50–59. https://doi.org/10.1016/j.eplepsyres.2018.04.005

Djukic, B., Casper, K. B., Philpot, B. D., Chin, L.-S., & McCarthy, K. D. (2007). Conditional Knock-out of Kir4.1 leads to glial membrane depolarization, inhibition of potassium and glutamate uptake, and enhanced short-term synaptic potentiation. *The Journal of Neuroscience*, *27*(42), 11354–11365. https://doi.org/10.1523/JNEUROSCI.0723-07.2007

Genoud, C., Houades, V., Kraftsik, R., Welker, E., & Giaume, C. (2015). Proximity of excitatory synapses and astroglial gap junctions in layer IV of the mouse barrel cortex. *Neuroscience*, *291*, 241–249. https://doi.org/10.1016/j.neuroscience.2015.01.051

Ghézali, G., Calvo, C.-F., Pillet, L.-E., Llense, F., Ezan, P., Pannasch, U., … Rouach, N. (2018). Connexin 30 controls astroglial polarization during postnatal brain development. *Development*, *145*(4), dev155275. https://doi.org/10.1242/dev.155275

Giaume, C., Koulakoff, A., Roux, L., Holcman, D., & Rouach, N. (2010). Astroglial networks: A step further in neuroglial and gliovascular interactions. *Nature Reviews. Neuroscience*, *11*(2), 87–99. https://doi.org/10.1038/nrn2757

Griemsmann, S., Höft, S. P., Bedner, P., Zhang, J., von Staden, E., Beinhauer, A., … Steinhäuser, C. (2015). Characterization of Panglial gap junction networks in the thalamus, neocortex, and hippocampus reveals a unique population of glial cells. *Cerebral Cortex (New York, N.Y.: 1991)*, *25*(10), 3420–3433. https://doi.org/10.1093/cercor/bhu157

Haj-Yasein, N. N., Jensen, V., Vindedal, G. F., Gundersen, G. A., Klungland, A., Ottersen, O. P., … Nagelhus, E. A. (2011). Evidence that compromised K+ spatial buffering contributes to the epileptogenic effect of mutations in the human kir4.1 gene (KCNJ10). *Glia*, *59*(11), 1635–1642. https://doi.org/10.1002/glia.21205

Harks, E. G. A., de Roos, A. D. G., Peters, P. H. J., de Haan, L. H., Brouwer, A., Ypey, D. L., … Theuvenet, A. P. R. (2001). Fenamates: A novel class of reversible gap junction blockers. *Journal of Pharmacology and Experimental Therapeutics*, *298*(3), 1033–1041. Retrieved from. http://jpet.aspetjournals.org/content/298/3/1033

Heinemann, U., Lux, H. D., & Gutnick, M. J. (1977). Extracellular free calcium and potassium during paroxysmal activity in the cerebral cortex of the cat. *Experimental Brain Research*, *27*(3–4), 237–243. https://doi.org/10.1007/BF00235500

Heinemann, U., & Dieter Lux, H. (1977). Ceiling of stimulus induced rises in extracellular potassium concentration in the cerebral cortex of cat. *Brain Research*, *120*(2), 231–249. https://doi.org/10.1016/0006-8993(77)90903-9

Henneberger, C., & Rusakov, D. A. (2012). Monitoring local synaptic activity with astrocytic patch pipettes. *Nature Protocols*, *7*(12), 2171–2179. https://doi.org/10.1038/nprot.2012.140

Karus, C., Mondragão, M. A., Ziemens, D., & Rose, C. R. (2015). Astrocytes restrict discharge duration and neuronal sodium loads during recurrent network activity. *Glia*, *63*(6), 936–957. https://doi.org/10.1002/glia.22793

Kofuji, P., & Newman, E. A. (2004). Potassium buffering in the central nervous system. *Neuroscience*, *129*(4), 1043–1054. https://doi.org/10.1016/j.neuroscience.2004.06.008

Larsen, B. R., Assentoft, M., Cotrina, M. L., Hua, S. Z., Nedergaard, M., Kaila, K., … MacAulay, N. (2014). Contributions of the Na^+/K^+-ATPase, NKCC1, and Kir4.1 to hippocampal K^+ clearance and volume responses. *Glia*, *62*(4), 608–622. https://doi.org/10.1002/glia.22629

Larsen, B. R., & MacAulay, N. (2014). Kir4.1-mediated spatial buffering of K+: Experimental challenges in determination of its temporal and quantitative contribution to K+ clearance in the brain. *Channels*, *8*(6), 544–550. https://doi.org/10.4161/19336950.2014.970448

Lux, H. D., & Neher, E. (1973). The equilibration time course of $[K^+]0$ in cat cortex. *Experimental Brain Research*, *17*(2), 190–205. https://doi.org/10.1007/BF00235028

Matyash, V., & Kettenmann, H. (2010). Heterogeneity in astrocyte morphology and physiology. *Brain Research Reviews*, *63*(1–2), 2–10. https://doi.org/10.1016/j.brainresrev.2009.12.001

Mazel, T., Sčimonová, Z., & Syková, E. (1998). Diffusion heterogeneity and anisotropy in rat hippocampus. *Neuroreport*, *9*(7), 1299–1304.

Meunier, C., Wang, N., Yi, C., Dallerac, G., Ezan, P., Koulakoff, A., … Giaume, C. (2017). Contribution of Astroglial Cx43 Hemichannels to the modulation of glutamatergic currents by D-serine in the mouse

prefrontal cortex. *Journal of Neuroscience*, *37*(37), 9064–9075. https://doi.org/10.1523/JNEUROSCI.2204-16.2017

Minge, D., Senkov, O., Kaushik, R., Herde, M. K., Tikhobrazova, O., Wulff, A. B., … Henneberger, C. (2017). Heparan sulfates support pyramidal cell excitability, synaptic plasticity, and context discrimination. *Cerebral Cortex*, *27*(2), 903–918. https://doi.org/10.1093/cercor/bhx003

Nagy, J. I., Patel, D., Ochalski, P. A. Y., & Stelmack, G. L. (1999). Connexin30 in rodent, cat and human brain: Selective expression in gray matter astrocytes, co-localization with connexin43 at gap junctions and late developmental appearance. *Neuroscience*, *88*(2), 447–468. https://doi.org/10.1016/S0306-4522(98)00191-2

Newman, E. A., Frambach, D. A., & Odette, L. L. (1984). Control of extracellular potassium levels by retinal glial cell K^+ siphoning. *Science (New York, N.Y.)*, *225*(4667), 1174–1175.

Pan, F., Mills, S. L., & Massey, S. C. (2007). Screening of gap junction antagonists on dye coupling in the rabbit retina. *Visual Neuroscience*, *24*(4), 609–618. https://doi.org/10.1017/S0952523807070472

Pannasch, U., Freche, D., Dallérac, G., Ghézali, G., Escartin, C., Ezan, P., … Rouach, N. (2014). Connexin 30 sets synaptic strength by controlling astroglial synapse invasion. *Nature Neuroscience*, *17*(4), 549–558. https://doi.org/10.1038/nn.3662

Pannasch, U., Vargová, L., Reingruber, J., Ezan, P., Holcman, D., Giaume, C., … Rouach, N. (2011). Astroglial networks scale synaptic activity and plasticity. *Proceedings of the National Academy of Sciences of the United States of America*, *108*(20), 8467–8472. https://doi.org/10.1073/pnas.1016650108

Ransom, C. B., Ransom, B. R., & Sontheimer, H. (2000). Activity-dependent extracellular K+ accumulation in rat optic nerve: The role of glial and axonal Na+ pumps. *The Journal of Physiology*, *522*(3), 427–442. https://doi.org/10.1111/j.1469-7793.2000.00427.x

Ransom, C. B., Ye, Z., Spain, W. J., & Richerson, G. B. (2017). Modulation of tonic GABA currents by Anion Channel and Connexin Hemichannel antagonists. *Neurochemical Research*, *42*(9), 2551–2559. https://doi.org/10.1007/s11064-017-2246-4

Rouach, N., Koulakoff, A., Abudara, V., Willecke, K., & Giaume, C. (2008). Astroglial metabolic networks sustain hippocampal synaptic transmission. *Science*, *322*(5907), 1551–1555. https://doi.org/10.1126/science.1164022

Rouach, N., Segal, M., Koulakoff, A., Giaume, C., & Avignone, E. (2004). Carbenoxolone blockade of neuronal network activity in culture is not mediated by an action on gap junctions. *The Journal of Physiology*, *553*(3), 729–745. https://doi.org/10.1113/jphysiol.2003.053439

Schevon, C., Ng, S., Cappell, J., Goodman, R., McKhann, G., Waziri, A., … Emerson, R. (2008). Microphysiology of epileptiform activity in human neocortex. *Journal of Clinical Neurophysiology*, *25*(6), 321–330. https://doi.org/10.1097/WNP.0b013e31818e8010

Seifert, G., Hüttmann, K., Binder, D. K., Hartmann, C., Wyczynski, A., Neusch, C., & Steinhäuser, C. (2009). Analysis of astroglial K+ channel expression in the developing hippocampus reveals a predominant role of the Kir4.1 subunit. *The Journal of Neuroscience*, *29*(23), 7474–7488. https://doi.org/10.1523/JNEUROSCI.3790-08.2009

Sibille, J., Pannasch, U., & Rouach, N. (2014). Astroglial potassium clearance contributes to short-term plasticity of synaptically evoked currents at the tripartite synapse. *The Journal of Physiology*, *592*(1), 87–102. https://doi.org/10.1113/jphysiol.2013.261735

Simard, M., Arcuino, G., Takano, T., Liu, Q. S., & Nedergaard, M. (2003). Signaling at the Gliovascular Interface. *Journal of Neuroscience*, *23*(27), 9254–9262. https://doi.org/10.1523/JNEUROSCI.23-27-09254.2003

Somjen, G. G. (2001). Mechanisms of spreading depression and hypoxic spreading depression-like depolarization. *Physiological Reviews*, *81*(3), 1065–1096. https://doi.org/10.1152/physrev.2001.81.3.1065

Strohschein, S., Hüttmann, K., Gabriel, S., Binder, D. K., Heinemann, U., & Steinhäuser, C. (2011). Impact of aquaporin-4 channels on K+ buffering and gap junction coupling in the hippocampus. *Glia*, *59*(6), 973–980. https://doi.org/10.1002/glia.21169

Syková, E., & Vargová, L. (2008). Extrasynaptic transmission and the diffusion parameters of the extracellular space. *Neurochemistry International*, *52*(1–2), 5–13. https://doi.org/10.1016/j.neuint.2007.04.007

Sypert, G. W., & Ward, A. A. (1974). Changes in extracellular potassium activity during neocortical propagated seizures. *Experimental Neurology*, *45*(1), 19–41. https://doi.org/10.1016/0014-4886(74)90097-1

Theis, M., Jauch, R., Zhuo, L., Speidel, D., Wallraff, A., Döring, B., … Willecke, K. (2003). Accelerated hippocampal spreading depression and enhanced locomotory activity in mice with astrocyte-directed inactivation of connexin43. *Journal of Neuroscience*, *23*(3), 766–776.

Tovar, K. R., Maher, B. J., & Westbrook, G. L. (2009). Direct actions of Carbenoxolone on synaptic transmission and neuronal membrane properties. *Journal of Neurophysiology*, *102*(2), 974–978. https://doi.org/10.1152/jn.00060.2009

Vessey, J. P., Lalonde, M. R., Mizan, H. A., Welch, N. C., Kelly, M. E. M., & Barnes, S. (2004). Carbenoxolone inhibition of voltage-gated ca channels and synaptic transmission in the retina. *Journal of Neurophysiology*, *92*(2), 1252–1256. https://doi.org/10.1152/jn.00148.2004

Wallraff, A., Köhling, R., Heinemann, U., Theis, M., Willecke, K., & Steinhäuser, C. (2006). The impact of astrocytic gap junctional coupling on potassium buffering in the hippocampus. *The Journal of Neuroscience*, *26*(20), 5438–5447. https://doi.org/10.1523/JNEUROSCI.0037-06.2006

Wellbourne-Wood, J., Rimmele, T. S., & Chatton, J.-Y. (2017). Imaging extracellular potassium dynamics in brain tissue using a potassium-sensitive nanosensor. *Neurophotonics*, *4*(1), 015002. https://doi.org/10.1117/1.NPh.4.1.015002

Wenzel, M., Hamm, J. P., Peterka, D. S., & Yuste, R. (2019). Acute focal seizures start as local synchronizations of neuronal ensembles. *Journal of Neuroscience*, *39*(43), 8562–8575. https://doi.org/10.1523/JNEUROSCI.3176-18.2019

Xiong, Z.-Q., & Stringer, J. L. (2000). Sodium pump activity, not glial spatial buffering, clears potassium after epileptiform activity induced in the dentate gyrus. *Journal of Neurophysiology*, *83*(3), 1443–1451. https://doi.org/10.1152/jn.2000.83.3.1443

Xu, L., Zeng, L.-H., & Wong, M. (2009). Impaired astrocytic gap junction coupling and potassium buffering in a mouse model of tuberous sclerosis complex. *Neurobiology of Disease*, *34*(2), 291–299. https://doi.org/10.1016/j.nbd.2009.01.010

Zhang, Y., & Barres, B. A. (2010). Astrocyte heterogeneity: An underappreciated topic in neurobiology. *Current Opinion in Neurobiology*, *20*(5), 588–594. https://doi.org/10.1016/j.conb.2010.06.005

Zsiros, V., & Maccaferri, G. (2005). Electrical coupling between interneurons with different excitable properties in the stratum Lacunosum-Moleculare of the juvenile CA1 rat hippocampus. *Journal of Neuroscience*, *25*(38), 8686–8695. https://doi.org/10.1523/JNEUROSCI.2810-05.2005

How to cite this article: Breithausen B, Kautzmann S, Boehlen A, Steinhäuser C, Henneberger C. Limited contribution of astroglial gap junction coupling to buffering of extracellular K^+ in CA1 stratum radiatum. *Glia*. 2020;68:918–931. https://doi.org/10.1002/glia.23751